ARTICLE

Coordination-Controlled C−C Coupling Products via *ortho*-Site C−H Activation

Xue Zhang,[†,||] Na Xue,[‡,||] Chao Li,[†,||] Na Li,[†] Hao Wang,[†] Nemanja Kocić,[§] Sumit Beniwal,[§] Krisztián Palotás,[⊥] Ruoning Li,[†] Qiang Xue,[†] Sabine Maier,*[,§] Shimin Hou,*[,†,‡] and Yongfeng Wang*[,†,¶]

[†]Key Laboratory for the Physics and Chemistry of Nanodevices, Department of Electronics, Peking University, Beijing 100871, China

[‡]Peking University Information Technology Institute (Tianjin Binhai), Tianjin 300450, China

[§]Department of Physics, Friedrich-Alexander University Erlangen-Nürnberg, Erwin-Rommel-Strasse 1, 91058 Erlangen, Germany

[⊥]Institute for Solid State Physics and Optics, Wigner Research Center for Physics, Hungarian Academy of Sciences, H-1525 Budapest, Hungary

[¶]Beijing Academy of Quantum Information Sciences, Beijing 100193, China

Ⓢ *Supporting Information*

ABSTRACT: The coordination-restricted *ortho*-site C−H bond activation and dehydrogenative homocoupling of 4,4′-(1,3-phenylene)dipyridine (1,3-BPyB) and 4,4′-(1,4-phenylene)dipyridine (1,4-BPyB) on different metal surfaces were studied by a combination of scanning tunneling microscopy, noncontact atomic force microscopy, and density functional theory calculations. The coupling products on Cu(111) exhibited certain configurations subject to the spatial restriction of robust two-fold Cu−N coordination bonds. Compared to the V-shaped 1,3-BPyB, the straight backbone of 1,4-BPyB helped to further reduce the variety of reactive products. By utilizing the three-fold coordination of Fe atoms with 1,4-BPyB molecules on Au(111), a large-scale network containing single products was constructed. Our results offer a promising protocol for controllable on-surface synthesis with the aid of robust coordination interactions.

KEYWORDS: C−H bond activation, dehydrogenative homocoupling, STM, coordination interaction, AFM
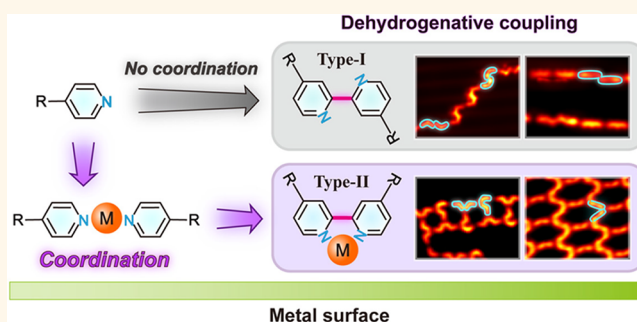
The C−C coupling induced by C−H bond activation is of vital importance in synthetic chemistry,[1−8] especially in aryl−aryl coupling because of the irreplaceable basic role of aryl groups in various aromatic compounds.[9−15] To trigger and accelerate the activation of originally inert C−H bonds, various strategies have been adopted such as transition-metal catalysis,[16−18] harsh conditions,[19] and metal supports.[20−23] Among them, chemical reactions on metal surfaces have drawn intensive attention in which the metal surface can act as a support and a catalyst simultaneously. The effectiveness of metal surfaces in chemocatalysis has been validated in different kinds of reactions,[24] for example, Ullmann coupling,[25−29] carbene intermediates,[30,31] arylalkyne cyclization,[32,33] and Glaser coupling.[34,35]

However, there are still great challenges such as accomplishing high selectivity among multiple reaction sites[36] and obtaining single-product configurations on the surface. The most common way to tackle the multisite issue is introducing directing groups and varying metal surfaces to achieve mono/diselective bond activation.[37] In contrast to regioselectivity, research aimed at the selectivity of product configuration is rarely reported. One feasible solution is to bring in an additional driving force so as to restrict the orientations of precursor molecules before new chemical bonds are formed. A self-assembly strategy driven by hydrogen bonds has been proved to steer on-surface reactions selectively.[38] The metal−organic coordination can display particular advantages owing to its intrinsic stability and the accessibility of metal atoms from either the substrate surface or codeposition. The robust coordination interaction is expected to generate spatial restriction on the coupling reaction.[39,40] Thus, by designing proper precursor molecules and coordination systems, it is

possible to achieve a highly ordered system made up by single products.

Herein, we report a coordination-restricted *ortho*-site C−H bond activation and dehydrogenative homocoupling of V-shaped and straight bispyridine molecules on different metal surfaces. Because of the significant spatial restriction effect of the robust coordination bonds, the configuration of final products can be selectively controlled and a single-product system can be realized by utilizing proper coordination interaction and precursor molecules of highly symmetrical backbone.

RESULTS AND DISCUSSION

Pyridyl molecules can undergo dehydrogenative coupling with the endmost pyridine groups as directing groups. The heat-induced C−H bond activation and dehydrogenative coupling are liable to occur at the *ortho* positions of pyridine groups. Owing to planar restriction of the metal substrate, two types of positioning modes (I and II) are anticipated, as shown in Figure 1a. Type-I is characterized by two homolateral nitrogen
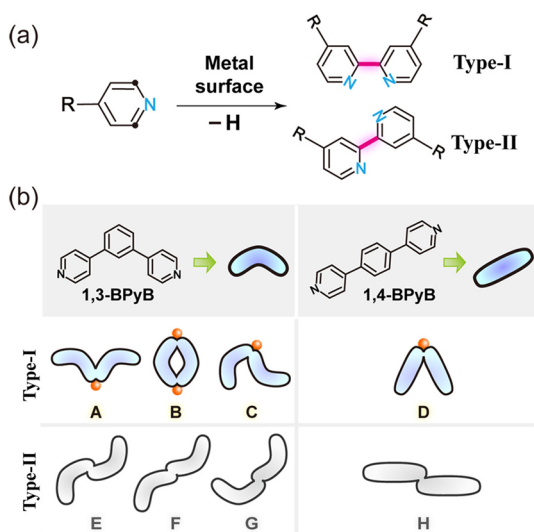

Figure 1. Scheme of selective C−H bond activation controlled by metal−organic coordination interaction. (a) C−H bond activation and dehydrogenative homocoupling occurring on the *ortho*-sites of a pyridine group. Two different types of products can be obtained considering planar restriction. (b) Two types of product configuration generalized from 1,3-BPyB and 1,4-BPyB. Products of type-I configurations can be selectively synthesized by the coordination-restricted effect.

atoms, which can coordinate to the same metal atom, while for type-II, the two nitrogen atoms are at opposite sides of the newly formed C−C covalent bond. With different molecular shapes, various product configurations can be derived from the two positioning types. Figure 1b gives two examples of precursor molecules with a bent and a straight shape, respectively. For the 1,3-BPyB molecule with 120° backbone, each type of the positioning mode leads to three different kinds of product configurations (A, B, C for type-I and E, F, G for type-II), regardless of the mirror symmetrical ones here. For the straight 1,4-BPyB molecule, there is only one kind of product for each mode (D for type-I and H for type-II).

Thus, the classification shown in Figure 1 provides an idea to selectively control the product configuration by elaborate predesign of the molecular shape and the bonding type

between reactant molecules. By utilizing the robust coordination interaction throughout the whole reaction process, products of type-I configurations can be tendentiously synthesized; by selecting precursor molecules of highly symmetrical backbones, the kinds of possible products can be further reduced.

On the basis of above strategy, we investigated the selective C−H bond activation reactions of 1,3-BPyB and 1,4-BPyB on Cu(111) by scanning tunneling microscopy (STM). When deposited at room temperature (RT), the V-shaped 1,3-BPyB molecules interact with Cu adatoms via two-fold coordination interaction[41−45] and form discrete closed rings on Cu(111) as reported previously.[46] When the sample is heated to a slightly higher temperature (320 K), a few distorted connected rings are observed as indicated by the cyan circles in Figure 2a.
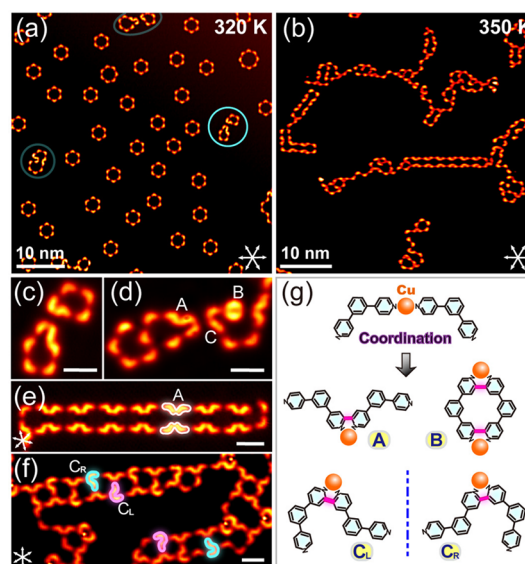

Figure 2. Coordination-restricted dehydrogenative coupling of 1,3-BPyB on Cu(111) and representative product structures. (a, b) STM images of 1,3-BPyB on Cu(111) after annealing at 320 and 350 K, respectively. The white arrows indicate equivalent [1$\bar{1}$0] direction. (c, d) Representative structures formed by molecular homocoupling inside coordinated rings. (e, f) Regular ribbon-like structures formed by different coupling products. (g) Schematic diagram illustrating the spatial restriction of the coordination bond on final product configuration. The length of scale bar in panels c−f equals to 2 nm. All STM images are acquired under constant-height mode and (a, b) $V_b = 10$ mV, $I_t = 51$ pA; (c−f) $V_b = 5$ mV, $I_t = 60$ pA.

Intact coordinated rings still dominate the whole surface at this temperature. After further annealing the sample at a temperature of 350 K, coordinated rings almost fully disappear and branched, irregular structures emerge, as shown in Figure 2b.

Figure 2c depicts the fine structures of the partly reacted rings marked by the cyan circle in Figure 2a. The shape of these distorted rings gives a hint to a reaction process in which the dehydrogenative homocoupling occurs under the restriction of aboriginal coordination bonds. The formation of coupling products can be affirmed by their smooth appearance. Besides, it is nearly impossible for two pristine 1,3-BPyB molecules to stay so close to each other due to the repulsive interaction between peripheral hydrogen atoms. The coupled 1,3-BPyB molecules look brighter than those pristine ones. Figure 2d shows an example of a highly disordered structure
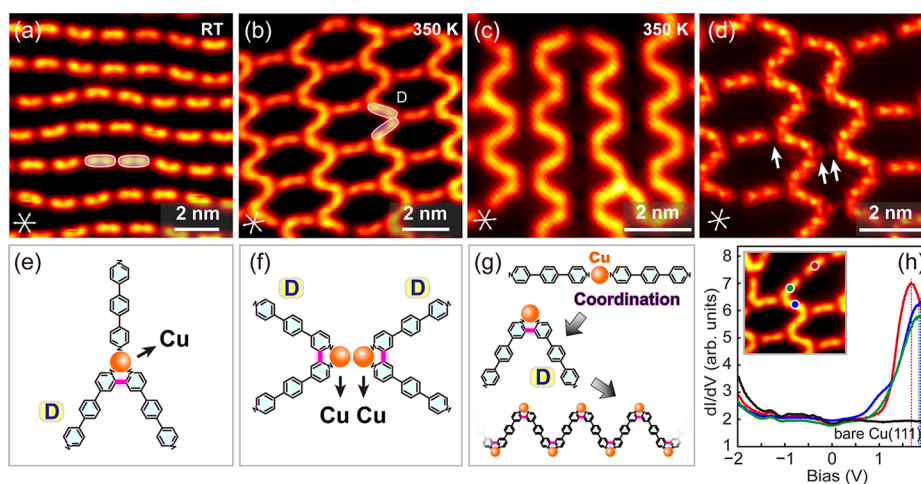
Figure 3. Coordination-restricted dehydrogenative coupling of 1,4-BPyB on Cu(111) at high coverage. (a) One-dimensional two-fold coordinated chains formed at RT. (b) Mixed honeycomb network made up by pristine 1,4-BPyB and covalently connected product D. (c) Structures entirely composed of polymers derived from product D. (d) STM image scanned using a tip modified with an adsorbed molecule. The coordinated Cu adatoms are clearly identified as bright protrusions and highlighted by white arrows. (e) Structural model of the coordinated trimer made up by one coupling product D and one pristine 1,4-BPyB. (f) Structural model of two head-to-head products D with two interstitial Cu adatoms. (g) Schematic diagram revealing the stepwise synthesis of product D and polymer with the aid of coordination interaction. (h) Differential conductance (dI/dV) spectra measured on pristine (red) and reacted (green and blue) 1,4-BPyB, respectively. The background spectrum (black) is measured on bare Cu(111) area. The forked arrows in panels a−d indicate equivalent [1$\bar{1}$0] direction. All the STM images were acquired under constant-height mode and (a) $V_b = 1$ mV, $I_t = 75$ pA; (b) $V_b = 1$ mV, $I_t = 90$ pA; (c) $V_b = 5$ mV, $I_t = 80$ pA; (d) $V_b = 0.01$ mV, $I_t = 156$ pA.

containing three kinds of products (A, B, and C) concurrently. Apart from aforementioned products that emerge after thermal activation, there are some interesting ribbon-like patterns as shown in Figures 2e and f. The chain in Figure 2e is formed entirely by the saddle-like products A as portrayed by the white contours. Each product A connects to its lateral neighbors via N−Cu−N coordination. Figure 2f shows a kind of compound structure constructed by regularly arranged product A and C. The contours of product C have been highlighted and discriminated by different colors according to adsorption-induced chirality on surface.

Notably, the dehydrogenative coupling products of 1,3-BPyB on Cu(111) exclusively possess type-I configuration, corroborating the important role of coordination interaction throughout the C−H bond activation and dehydrogenative coupling process. Because of the restriction effect of the robust coordination bond, the two N atoms are always kept on the same side and coordinating to the same Cu adatom in type-I configuration. Figure 2g concretes the dominating impact of coordination interaction on final product configuration.

Although the products are restricted to coordination-inclined configurations, there are still various product structures due to the bent molecular shape of 1,3-BPyB. It remains difficult to separate different kinds of coexisted products. Besides, it is impractical to increase the reaction temperature or extend the duration of heating owing to the significant desorption rate of molecules. To pursue the ultimate goal of a single-product system, it is necessary to reduce the kinds of products from the origin. For this purpose, 1,4-BPyB with straight and symmetrical molecular skeleton is employed. Without thermal activation, 1,4-BPyB molecules assemble into one-dimensional coordinated chains on Cu(111) through robust two-fold N−Cu−N coordination, as displayed in Figure 3a. After the sample was heated to 350 K, the C−H bond activation and covalent coupling were triggered, and as expected, only product D was obtained because of the

restriction effect of the coordination bond. The distorted honeycomb-like network in Figure 3b is made up of pristine 1,4-BPyB and product D with prevailed three-fold coordination. One unreacted 1,4-BPyB molecule is stabilized by two products D in the form of three-fold coordination. Products D interplay with each other by secondary dehydrogenative coupling, forming a snake-like polymer. Structures fully composed of such covalent polymers are occasionally observed as shown in Figure 3c; however, on a much smaller scale compared to the combined network in Figure 3b due to the intrinsic irreversibility and low diffusion ability of covalent bond.

To corroborate the involvement of coordinated Cu adatoms, a molecule-functionalized STM tip was utilized for imaging. The appearance of the coordinated Cu adatoms can be clearly identified by the bright protrusions in Figure 3d, indicated with white arrows. There is one coordinated Cu adatom connecting a pristine 1,4-BPyB and a product D in a three-fold coordination node, and two adjacent Cu adatoms bridging two opposite products D of neighboring polymers. Structural models of a coordination trimer and two opposite products D with two interstitial Cu adatoms are presented in Figures 3e and f, respectively. Figure 3g illustrates the reaction process of 1,4-BPyB from coordinated dimer to single-product D, then to the final covalent polymer, which can act as the building block for ordered covalent network like those shown in Figure 3b and c. Scanning tunneling spectroscopy (STS) measurements reveal molecular unoccupied states for pristine and reacted 1,4-BPyB, respectively. As shown in Figure 3h, the lowest unoccupied molecular orbital (LUMO) for a pristine 1,4-BPyB is measured to be about 1.7 eV (red curve), while after dehydrogenative coupling the LUMO shifts to ∼1.9 eV (green and blue curves).

Series of dI/dV maps were also recorded under varied sample voltages to investigate the electronic features of dehydrogenative coupling structures. As depicted in Figure 4,
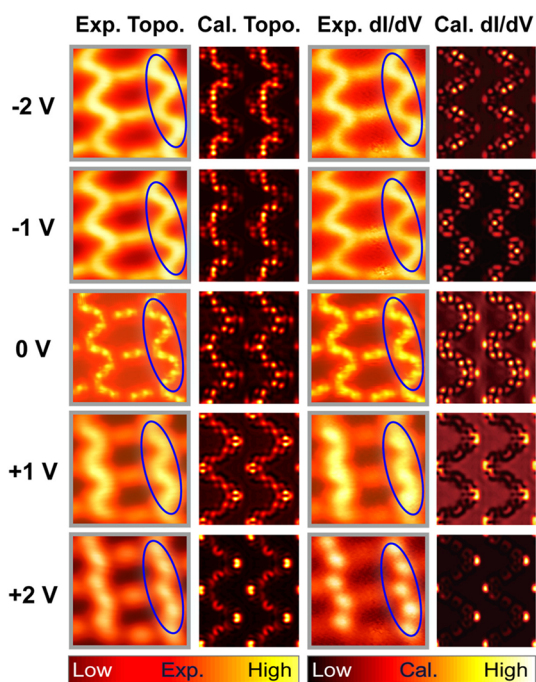
Figure 4. Experimental and calculated topographs and dI/dV maps of coupling structures formed by 1,4-BPyB on Cu(111). The calculated results (labeled by Cal.) agree well with experimental observations (labeled by Exp.) that the coordinated nodes of a marked polymer appear much brighter than the rest part at large positive voltages. All the experimental and calculated topographs and dI/dV maps are acquired under constant-height mode.

the topographs (labeled by Topo.) and the dI/dV maps (labeled by dI/dV) acquired on a part of the coupling honeycomb network are featureless at negative sample voltages. As the voltage becomes more positive, the coordinated nodes of the polymer (indicated by blue circles) appear much brighter than the rest. By contrast, the pristine 1,4-BPyB molecule has much dimmer contour in both STM images and dI/dV maps at 1 and 2 V. Identical tendency is observed in simulated topographs and dI/dV maps of a polymer fragment using bSKAN-VASP code.[47,48] This corroborates the models we put forward with in Figure 3g. To be noted, more details can be observed in our simulated topographic and dI/dV maps than in the experimental images. This is because that the tip is approximated as an atom and only s orbital is considered. For a real tip, it usually has complicated shape and its electric configuration may contain s, d, p orbitals, which would lead to reduced resolution in the experimental images.

The formation of a covalent bond between *ortho*-site carbons of neighboring molecules after C−H bond activation was verified by performing noncontact atomic force microscopy (nc-AFM) measurements, as shown in Figure 5. CO molecules were codeposited onto the Cu(111) surface to form a CO-modified tip, as shown in Figure 5a. After picking up a single CO molecule onto the tip apex,[49,50] the newly formed C−C bonds were unambiguously observed from the nc-AFM frequency shift image (Figures 5b and S3). The sharp homogeneous line in the nc-AFM image that connects two pyridine groups (see white arrow Figure 5d) clearly indicates a additional C−C bond between neighboring molecules, while the Cu adatom in the coordination bond does not show a pronounced contrast (see green and yellow arrow in Figure
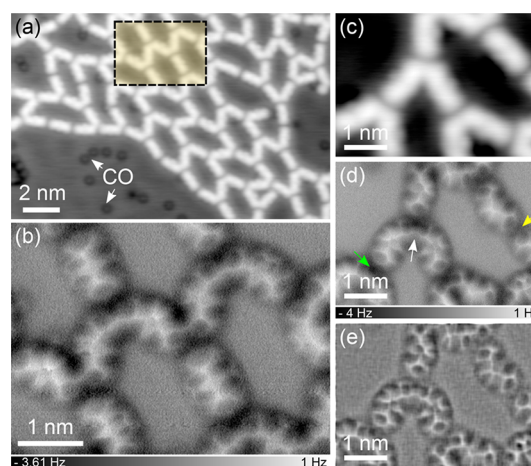

Figure 5. STM topographic and nc-AFM frequency shift image of the coupling product on Cu(111) after annealing to 400 K. (a) Constant-current STM image of the coupled network and codeposited CO molecules. (b) Nc-AFM frequency shift image of the area marked by dashed square in panel a. (c) Constant-current overview image with the corresponding (d) nc-AFM image and (e) Laplace filtered nc-AFM image revealing the different bonding schemes in detail: covalent C−C bond (white arrow), three-fold Cu coordination (green arrow), and two-fold Cu coordination (yellow arrow). All STM images are measured with a CO-functionalized tip. Scanning parameters: (a, c) V_b = 30 mV, I_t = 14 pA; (b, d) The tip is 10 pm retracted relative to a STM set point of 30 mV and 14 pA on the bare Cu.

5d). The distortions observed at the central carbon rings of the molecule are caused by frustrated rotations of the corresponding ring.[51] Mechanical manipulation was also employed to confirm the formation of a covalent C−C bond as demonstrated in Figure S1. An initially fixed product D in a two-fold coordinated chain could be peeled off intactly by a STM tip and moved individually, indicating the formation of robust covalent bond within product D.

The surface-assisted C−H bond activation on the *ortho*-site of a pyridyl molecule was confirmed by density functional theory (DFT) calculations with climbing image nudged-elastic band (CI-NEB) method. As shown in Figure 6, a single pyridine ring with one fixed (marked by a blue circle) and one free Cu adatom (marked by a yellow circle) is set as the initial state (IS). During the C−H bond activation process, the fixed Cu adatom always keeps coordinating to the N atom, while the free Cu adatom gradually approaches the *ortho*-H atom and finally cuts it off from the *ortho*-site (final state, FS). The variation of the molecular configuration and the path of the additional free Cu adatom can be clearly identified in Figure 6a. The reaction barrier between neighboring immediate states is illustrated in Figure 6b. The IS transforms into the first transition state 1 experiencing an energy barrier of 0.14 eV. The second transition state (state 3) is reached by overcoming a barrier of 1.28 eV from the immediate state 2. Then the FS is achieved by an energy relaxation of 1.16 eV from the transition state 3. Once the barrier of C−H dissociation is overcome, the Cu−C bond dissociation would occur with a much lower energy barrier of 0.76 eV (Figure S5) and a subsequent spontaneous C−C coupling follows.

To study the role of a coordinated Cu adatom extensively, the reaction path with only a free Cu adatom and no coordinated adatom was calculated as a comparison, as given in Figure S2. In this case, the barrier for dehydrogenation is about
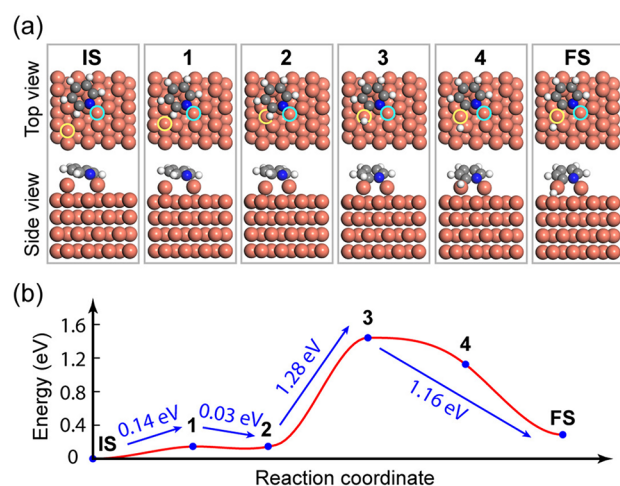
Figure 6. DFT calculations about the *ortho*-site C−H bond activation process of a single pyridine ring on Cu(111). (a) Top and side view of molecular configuration and adatom position throughout the C−H bond activation process. The pyridine ring keeps coordinating to one Cu adatom, while the other free Cu adatom migrates to remove the *ortho*-H atom. (b) Calculated reaction barrier between different immediate sates in the dehydrogenation process.
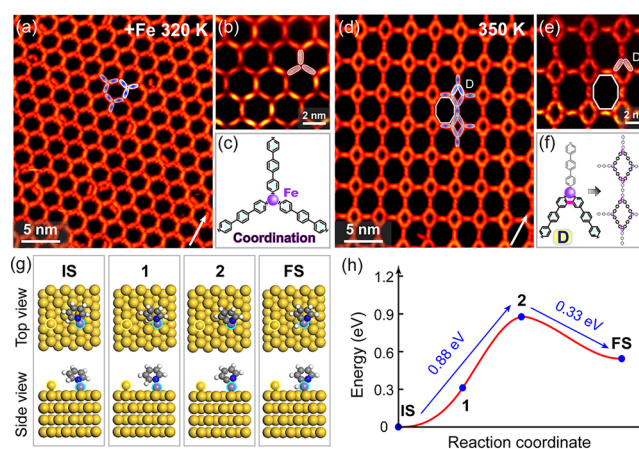

Figure 7. Coordination-restricted dehydrogenative coupling of 1,4-BPyB on Au(111) with coordinated Fe atoms. (a) Coordinated honeycomb network formed by three-fold coordination of 1,4-BPyB and Fe atoms. (b) Detailed STM image of the coordinated network. (c) Molecular model of a coordinated trimer. (d) Compound network emerging after triggering the dehydrogenative coupling at 350 K. Such network is composed of well-organized pristine 1,4-BPyB and product D through three-fold coordination interaction. (e) Close-up image showing details of the compound network of octagonal cavities in panel d. The contour of a product D has been marked in white. (f) Schematic diagram interpreting the molecular structure of product D and the formation of compound network with D as the only product. (g, h) Calculated reaction path and energies of different intermediate states based on a pyridine ring on Au(111) with one coordinated Fe atom and one free Au adatom. The white arrows in panels a and d point to $[1\bar{1}0]$ direction. Scanning parameters: (a, d) constant-current mode, V_b = 0.5 V, I_t = 30 pA; (b) constant-height mode, V_b = 50 mV, I_t = 60 pA; (e) constant-height mode, V_b = 10 mV, I_t = 70 pA.

1.27 eV, nearly the same as when the coordinated Cu adatom is present. It points out the fact that the coordinated Cu adatom has little influence on changing the dehydrogenation barrier, and only the free Cu adatom plays the role of catalyst. The exclusive effect of a coordinated Cu adatom is to anchor the steric configuration of precursor molecules. When considering the stray hydrogen atoms,[52−54] the calculated barrier reduces to 0.65 eV (Figure S7). The calculation well explains why the C−H activation can happen at the rather low temperature.

Utilizing the spatial restriction effect of coordination bonds and precursors of highly symmetrical structures, the kinds of product configurations have been greatly reduced in the 1,4-BPyB/Cu(111) system. However, inhomogeneities of the final product structure still exist as the length of polymer is random and hard to control. Therefore, it is not strictly a system of single-product. Besides, the stiffness of the long covalent backbone of the polymer may hinder the formation of large-sized ordered network.

To improve the overall orderliness of the final product structure, based on the above considerations, the secondary C−H bond activation on the ends of product D should be suppressed and the occurrence of polymers should be reduced. Therefore, the strong catalytic Cu(111) surface was replaced with the relatively inert Au(111) surface, and more robust three-fold N−Fe coordination was employed to counteract the severe molecular desorption. Following the route designed above, 1,4-BPyB and Fe atoms were codeposited onto Au(111) and preheated to 320 K to realize sufficient coordination before C−H bond activation. A large-scale honeycomb network was constructed with Fe−N coordination interaction[55−57] and a coordinated trimer as the basic unit is presented in Figures 7a and b. The molecular model of a coordinated trimer is demonstrated in Figure 7c. After the coordinated network is annealed at 350 K, a distinct phase appears, as shown in Figure 7d. From the close-up of Figure 7e, it is identified that such a network with octagonal cavities

consists of regularly mixed pristine 1,4-BPyB and products D. In contrast to the coupling network in Figure 3b on Cu(111), the products D here are completely intact individuals and no undesired polymer is found. Pristine 1,4-BPyB and product D are all stabilized by three-fold N−Fe coordination. Figure 7g and h display the reaction path calculated by CI-NEB method, in which the pyridyl ring on Au(111) surface keeps coordinating to a Fe atom (marked by a blue circle) with a free Au adatom (marked by yellow circle) aside. The calculated dehydrogenation barrier is about 0.88 eV. Different from the case of Cu(111), the dehydrogenation process does not require help from the additional Au adatom and could occur with only a coordinated Fe atom. The calculated barrier increases to 1.59 eV without the Fe atom (Figure S6).

From the DFT calculations in Figures 6a and 7g, it could be recognized clearly that the targeted pyridyl C−H bond is pulled down toward the metal adatom, leading to a reduced C−H dissociation barrier. Similar "pulling effect" has been reported in other C−H activation-related studies. For example, in the *ortho*-site coupling of phenol derivatives, the phenol group has to tilt away from the surface first to allow the approaching of a metal adatom to *ortho*-site C−H bond and then be pulled down toward surface due to the interaction of the *ortho*-site carbon radical with the metal adatom.[37] For the case where metal adatom is absent, the targeted C−H bond is pulled down directly toward surface through interactions of adjacent radical sites with surface atoms.[58] Therefore, the approximation of molecules toward catalyzing metal adatoms or surface atoms is critical to facilitate aromatic C−H bond

activation, despite the dependence of particular approach on the initial precursor state and actual reaction environment.

The evolution of product configuration in the absence of spatial restriction from coordination bond was studied as a contrast. The selectivity induced by aforehand hydrogen-bonded self-assembly structures has been observed in Ullmann Coupling process.[38] The two molecules studied both self-assemble into close-packed islands on Au(100) surface at RT. The basic unit is windmill-like hydrogen-bonded tetramer, as shown in Figures 8a and f. The sizes of unit cells marked by
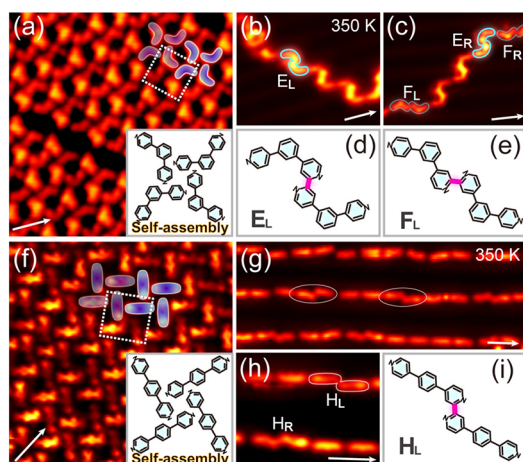

Figure 8. Structure transformations of 1,3-BPyB and 1,4-BPyB on Au(100) from self-assembly to dehydrogenative coupling. (a) 1,3-BPyB self-assembles into close-packed island with hydrogen-bonded tetramers as building blocks. The inset gives the model of a hydrogen-bonded tetramer. (b, c) Dehydrogenative coupling structures of 1,3-BPyB after annealed at 350 K. Products E and F have been highlighted with cyan contours. (d, e) Molecular models of product E and F. (f) Close-packed island formed by self-assembly of 1,4-BPyB. The basic unit is still the hydrogen-bonded tetramer with its molecular model shown in the inset. (g) STM image demonstrating the results after annealing the structure (f) at 350 K. Most of the 1,4-BPyB molecules are unreacted and stabilized by two-fold coordination with Au adatoms, fabricating one-dimensional coordinated chains. A few coupling products H are found interspersed in the coordinated chains as circled. (h) Close-up of products H with opposite chirality. (i) Molecular model of product H. The white arrows point to the [011] direction and stand for 2 nm. Scanning parameters: constant-height mode, (a) $V_b = 10$ mV, $I_t = 100$ pA; (b, c) $V_b = 10$ mV, $I_t = 80$ pA; (f) $V_b = 100$ mV, $I_t = 70$ pA; (g) $V_b = 10$ mV, $I_t = 90$ pA; (h) $V_b = 3$ mV, $I_t = 120$ pA.

white dashed squares are measured to be 2.2 and 2.1 nm, respectively. Identical hydrogen-bonded tetramer islands formed by 1,3-BPyB and by 1,4-BPyB can be acquired on Au(111) as well. However, almost all molecules desorb before the desired C−H bond activation could occur. By contrast, a few coupling products are able to survive on Au(100) owing to stronger molecule−substrate interaction than that on Au(111). Representative results after annealing the sample at 350 K are shown in Figure 8b and c, and g and h. As expected, products of type-II configuration emerge for both 1,3-BPyB (Figure 8b,c) and 1,4-BPyB (Figure 8g,h) for the lack of sufficient spatial restricting force like that offered by a coordination bond.

Moreover, these products with type-II configuration are found to show size matching with substrate lattice. Figure 8d,

e, and i depict the corresponding molecular models of product E, F and H, respectively. The size of product E fits the distance between neighboring reconstructed ridges of Au(100); the backbone of product F and H is aligned along the reconstructed direction of Au(100). Except for the coupling products, great amounts of pristine 1,3- and 1,4-BPyB are stabilized by two-fold N−Au coordination due to the significant increase of Au adatoms after thermal activation. Most of the one-dimensional coordinated chains align along the [011] reconstructed direction of Au(100) surface. Notably, no product G is found for 1,3-BPyB on Au surface. The highly asymmetrical structure and the mismatch of size and orientation toward the surface are assumed to be responsible. Further annealing causes complete molecular desorption in our experiment. To highlight the effectivity of coordination bond in terms of controlling product configuration, we compared the yields of type-I and II products in both coordination and noncoordination systems as shown in Figure S4. In a coordination system, type-I products are overwhelming, while in a deficient coordination system, the two types of products coexist and no selectivity is found.

CONCLUSIONS

In summary, we studied the influence of coordination interaction and self-assembly on final product configuration in *ortho*-site C−H bond activation and dehydrogenative homocoupling of pyridyl molecules on metal surfaces. Assisted STS measurements, mechanical manipulation, nc-AFM, and DFT calculations were performed to verify the formation of the coupling product. Because of the spatial restriction effect of robust N−Cu−N coordination bonds during the whole reaction process on Cu(111), only those configurations that allow a coordinated Cu adatom to stay between two pyridine groups can be formed. The varieties of product configuration could be further reduced by using precursor molecules of highly symmetrical shape. Moreover, by choosing coordination interaction of appropriate coordination number and inert metal surface, a large-scale ordered compound network containing only one kind of coupling product was constructed utilizing 1,4-BPyB of straight backbone and three-fold Fe−N coordination on Au(111). Our findings unveil the vital influence of coordination interaction on product configurations in terms of selective C−H bond activation, which is promising for controllable on-surface synthesis.

METHODS

STM Experiments. Sample preparation and measurements were performed in an ultrahigh vacuum LT-STM system (Unisoku) equipped with standard surface preparation facilities. The Cu(111), Au(111), and Au(100) substrates were prepared by cycles of Ar⁺ sputtering and annealing. The commercial 1,3-BPyB and 1,4-BPyB molecules were deposited onto the metal substrates from homemade tantalum crucibles. Fe atoms were sublimated from Knudsen crucible at about 1500 K. The substrates were kept at room temperature during deposition of molecules and Fe atoms. The duration of reaction was 10 min unless stated otherwise. The vacuum was maintained in the order of 10^{-10} Torr during molecular deposition and subsequent imaging. All STM images were acquired at 4 K using a sharpened Pt/Ir tip.

AFM Experiments. The nc-AFM measurement was carried out with a low-temperature STM/AFM (Scienta-Omicron

GmbH) in combination with the Nanonis control electronics (SPECS GmbH). The instrument was housed in a two-chamber ultrahigh vacuum (UHV) system equipped with a separate preparation chamber (base pressure below 10^{-10} mbar). All AFM images were acquired in constant-height mode at 4.3 K. Commercial qPlus tuning fork sensors (Scienta-Omicron GmbH) with a chemically etched tungsten tip were used (resonance frequency $f_0 \approx 21.255$ kHz, $Q \approx 10\,000$, and $A_{osc} = 80$ pm). To achieve submolecular resolution, the tip apex was functionalized with a single CO molecule. The tuning fork was grounded, and the applied bias voltages refer to the sample. For AFM imaging, a small offset gap voltage (<1 mV) was used to minimize the tunneling current.

DFT Calculations. DFT calculations were performed with climbing image nudged-elastic band (CI-NEB) method by using the 5.3.5 version of the Vienna *Ab initio* Simulations Package (VASP).[59−61] The core electrons were described by the pseudopotentials constructed according to the projector augmented wave (PAW) method.[62] The exchange−correlation energy was calculated with the opt-B88 functional[63−65] to take into account the van der Waals (vdW) dispersive correction. The Cu(111) and Au(111) surface was modeled by a slab of 64 atoms composed by four atomic layers. The supercell containing molecule-slab has a dimension of 10.27 Å × 8.89 Å × 22.01 Å and 11.77 Å × 11.77 Å × 22.01 Å, respectively. A 3 × 3 × 1 Monkhorst−Pack grid was used for the Brillouin zone sampling. Simulations of STM images and dI/dV maps were performed on a periodic polymer fragment using bSKAN code[47,48] based on VASP. A supercell containing an intact product D and two coordinated Cu adatoms was built to construct the periodic polymer according to experimental results.

ASSOCIATED CONTENT

Ⓢ **Supporting Information**

The Supporting Information is available free of charge on the ACS Publications website at DOI: 10.1021/acsnano.8b06885.

> Details of tip manipulations; additional nc-AFM measurements; relative ratio of different products in coordination and noncoordination systems; supplementary DFT calculations (PDF)

AUTHOR INFORMATION

Corresponding Authors
*E-mail: sabine.maier@fau.de.
*E-mail: smhou@pku.edu.cn.
*E-mail: yongfengwang@pku.edu.cn.

ORCID Ⓘ

Na Li: 0000-0001-6924-8387
Sumit Beniwal: 0000-0002-9381-5481
Krisztián Palotás: 0000-0002-1914-2901
Sabine Maier: 0000-0001-9589-6855
Shimin Hou: 0000-0002-5042-4405
Yongfeng Wang: 0000-0002-8171-3189

Author Contributions
‖These authors contributed equally to this paper.

Notes
The authors declare no competing financial interest.

REFERENCES

(1) Ahmed, J.; Sreejyothi, P.; Vijaykumar, G.; Jose, A.; Raj, M.; Mandal, S. K. A New Face of Phenalenyl-Based Radicals in the Transition Metal-Free C−H Arylation of Heteroarenes at Room Temperature: Trapping the Radical Initiator *via* C−C σ-Bond Formation. *Chem. Sci.* **2017**, *8*, 7798−7806.

(2) Schwach, P.; Pan, X.; Bao, X. Direct Conversion of Methane to Value-Added Chemicals over Heterogeneous Catalysts: Challenges and Prospects. *Chem. Rev.* **2017**, *117*, 8497−8520.

(3) Chiusoli, G. P.; Catellani, M.; Costa, M.; Motti, E.; Della Ca', N.; Maestri, G. Catalytic C−C Coupling through C−H Arylation of Arenes or Heteroarenes. *Coord. Chem. Rev.* **2010**, *254*, 456−469.

(4) He, Y.; Garnica, M.; Bischoff, F.; Ducke, J.; Bocquet, M.-L.; Batzill, M.; Auwärter, W.; Barth, J. V. Fusing Tetrapyrroles to Graphene Edges by Surface-Assisted Covalent Coupling. *Nat. Chem.* **2016**, *9*, 33−38.

(5) Zhong, D.; Franke, J.-H.; Podiyanachari, S. K.; Blömker, T.; Zhang, H.; Kehr, G.; Erker, G.; Fuchs, H.; Chi, L. Linear Alkane Polymerization on a Gold Surface. *Science* **2011**, *334*, 213−216.

(6) Guo, X.; Fang, G.; Li, G.; Ma, H.; Fan, H.; Yu, L.; Ma, C.; Wu, X.; Deng, D.; Wei, M.; Tan, D.; Si, R.; Zhang, S.; Li, J.; Sun, L.; Tang, Z.; Pan, X.; Bao, X. Direct, Nonoxidative Conversion of Methane to Ethylene, Aromatics, and Hydrogen. *Science* **2014**, *344*, 616−619.

(7) Sun, K.; Chen, A.; Liu, M.; Zhang, H.; Duan, R.; Ji, P.; Li, L.; Li, Q.; Li, C.; Zhong, D.; Müllen, K.; Chi, L. Surface-Assisted Alkane Polymerization: Investigation on Structure−Reactivity Relationship. *J. Am. Chem. Soc.* **2018**, *140*, 4820−4825.

(8) Xiang, F.; Gemeinhardt, A.; Schneider, M. A. Competition between Dehydrogenative Organometallic Bonding and Covalent Coupling of an Unfunctionalized Porphyrin on Cu (111). *ACS Nano* **2018**, *12*, 1203−1210.

(9) Cai, J.; Ruffieux, P.; Jaafar, R.; Bieri, M.; Braun, T.; Blankenburg, S.; Muoth, M.; Seitsonen, A. P.; Saleh, M.; Feng, X.; Müllen, K.; Fasel, R. Atomically Precise Bottom-Up Fabrication of Graphene Nanoribbons. *Nature* **2010**, *466*, 470−473.

(10) Ruffieux, P.; Wang, S.; Yang, B.; Sánchez-Sánchez, C.; Liu, J.; Dienel, T.; Talirz, L.; Shinde, P.; Pignedoli, C. A.; Passerone, D.; Dumslaff, T.; Feng, X.; Müllen, K.; Fasel, R. On-Surface Synthesis of Graphene Nanoribbons with Zigzag Edge Topology. *Nature* **2016**, *531*, 489−492.

(11) Treier, M.; Pignedoli, C. A.; Laino, T.; Rieger, R.; Müllen, K.; Passerone, D.; Fasel, R. Surface-Assisted Cyclodehydrogenation Provides a Synthetic Route towards Easily Processable and Chemically Tailored Nanographenes. *Nat. Chem.* **2011**, *3*, 61−67.

(12) Otero, G.; Biddau, G.; Sánchez-Sánchez, C.; Caillard, R.; López, M. F.; Rogero, C.; Palomares, F. J.; Cabello, N.; Basanta, M. A.; Ortega, J.; Méndez, J.; Echavarren, A. M.; Pérez, R.; Gómez-Lor, B.; Martín-Gago, J. A. Fullerenes from Aromatic Precursors by Surface-Catalysed Cyclodehydrogenation. *Nature* **2008**, *454*, 865−868.

(13) Sun, Q.; Zhang, C.; Kong, H.; Tan, Q.; Xu, W. On-Surface Aryl−Aryl Coupling *via* Selective C−H Activation. *Chem. Commun.* **2014**, *50*, 11825−11828.

(14) Cirera, B.; Giménez-Agulló, N.; Björk, J.; Martínez-Peña, F.; Martin-Jimenez, A.; Rodriguez-Fernandez, J.; Pizarro, A. M.; Otero, R.; Gallego, J. M.; Ballester, P.; Galan-Mascaros, J. R.; Ecija, D. Thermal Selectivity of Intermolecular *versus* Intramolecular Reactions on Surfaces. *Nat. Commun.* **2016**, *7*, 11002.

(15) Kocić, N.; Liu, X.; Chen, S.; Decurtins, S.; Krejčí, O.; Jelínek, P.; Repp, J.; Liu, S.-X. Control of Reactivity and Regioselectivity for On-Surface Dehydrogenative Aryl−Aryl Bond Formation. *J. Am. Chem. Soc.* **2016**, *138*, 5585−5593.

(16) Shang, R.; Ilies, L.; Nakamura, E. Iron-Catalyzed C−H Bond Activation. *Chem. Rev.* **2017**, *117*, 9086−9139.

(17) He, J.; Wasa, M.; Chan, K. S.; Shao, Q.; Yu, J.-Q. Palladium-Catalyzed Transformations of Alkyl C−H Bonds. *Chem. Rev.* **2017**, *117*, 8754−8786.

(18) Colby, D. A.; Bergman, R. G.; Ellman, J. A. Rhodium-Catalyzed C−C Bond Formation *via* Heteroatom-directed C−H Bond Activation. *Chem. Rev.* **2010**, *110*, 624−655.

(19) Arndtsen, B. A.; Bergman, R. G.; Mobley, T. A.; Peterson, T. H. Selective Intermolecular Carbon−Hydrogen Bond Activation by Synthetic Metal Complexes in Homogeneous Solution. *Acc. Chem. Res.* **1995**, *28*, 154−162.

(20) Yin, L.; Liebscher, J. Carbon−Carbon Coupling Reactions Catalyzed by Heterogeneous Palladium Catalysts. *Chem. Rev.* **2007**, *107*, 133−173.

(21) Haq, S.; Hanke, F.; Sharp, J.; Persson, M.; Amabilino, D. B.; Raval, R. Versatile Bottom-Up Construction of Diverse Macromolecules on a Surface Observed by Scanning Tunneling Microscopy. *ACS Nano* **2014**, *8*, 8856−8870.

(22) Wiengarten, A.; Seufert, K.; Auwärter, W.; Ecija, D.; Diller, K.; Allegretti, F.; Bischoff, F.; Fischer, S.; Duncan, D. A.; Papageorgiou, A. C.; Klappenberger, F.; Acres, R. G.; Ngo, T. H.; Barth, J. V. Surface-Assisted Dehydrogenative Homocoupling of Porphine Molecules. *J. Am. Chem. Soc.* **2014**, *136*, 9346−9354.

(23) Eichhorn, J.; Heckl, W. M.; Lackinger, M. On-Surface Polymerization of 1,4-Diethynylbenzene on Cu (111). *Chem. Commun.* **2013**, *49*, 2900−2902.

(24) Björk, J.; Hanke, F. Towards Design Rules for Covalent Nanostructures on Metal Surfaces. *Chem. - Eur. J.* **2014**, *20*, 928−934.

(25) Fan, Q.; Wang, C.; Han, Y.; Zhu, J.; Kuttner, J.; Hilt, G.; Gottfried, J. M. Surface-Assisted Formation, Assembly, and Dynamics of Planar Organometallic Macrocycles and Zigzag Shaped Polymer Chains with C−Cu−C Bonds. *ACS Nano* **2014**, *8*, 709−718.

(26) Lafferentz, L.; Eberhardt, V.; Dri, C.; Africh, C.; Comelli, G.; Esch, F.; Hecht, S.; Grill, L. Controlling On-Surface Polymerization by Hierarchical and Substrate-directed Growth. *Nat. Chem.* **2012**, *4*, 215−220.

(27) Bieri, M.; Nguyen, M.-T.; Gröning, O.; Cai, J.; Treier, M.; Aït-Mansour, K.; Ruffieux, P.; Pignedoli, C. A.; Passerone, D.; Kastler, M.; Müllen, K.; Fasel, R. Two-Dimensional Polymer Formation on Surfaces: Insight into the Roles of Precursor Mobility and Reactivity. *J. Am. Chem. Soc.* **2010**, *132*, 16669−16676.

(28) Liu, W.; Luo, X.; Bao, Y.; Liu, Y. P.; Ning, G.-H.; Abdelwahab, I.; Li, L.; Nai, C. T.; Hu, Z. G.; Zhao, D.; Liu, B.; Quek, S. Y.; Loh, K. P. A Two-Dimensional Conjugated Aromatic Polymer *via* C−C Coupling Reaction. *Nat. Chem.* **2017**, *9*, 563−570.

(29) Lackinger, M. Surface-Assisted Ullmann Coupling. *Chem. Commun.* **2017**, *53*, 7872−7885.

(30) Matena, M.; Stöhr, M.; Riehm, T.; Björk, J.; Martens, S.; Dyer, M. S.; Persson, M.; Lobo-Checa, J.; Müller, K.; Enache, M.; Wadepohl, H.; Zegenhagen, J.; Jung, T. A.; Gade, L. H. Aggregation and Contingent Metal/Surface Reactivity of 1,3,8,10-Tetraazaperopyrene (TAPP) on Cu (111). *Chem. - Eur. J.* **2010**, *16*, 2079−2091.

(31) Matena, M.; Riehm, T.; Stöhr, M.; Jung, T. A.; Gade, L. H. Transforming Surface Coordination Polymers into Covalent Surface Polymers: Linked Polycondensed Aromatics Through Oligomeriza-

tion of N-Heterocyclic Carbene Intermediates. *Angew. Chem.* **2008**, *120*, 2448−2451.

(32) Liu, J.; Ruffieux, P.; Feng, X.; Müllen, K.; Fasel, R. Cyclotrimerization of Arylalkynes on Au (111). *Chem. Commun.* **2014**, *50*, 11200−11203.

(33) Sun, Q.; Zhang, C.; Li, Z.; Kong, H.; Tan, Q.; Hu, A.; Xu, W. On-Surface Formation of One-Dimensional Polyphenylene Through Bergman Cyclization. *J. Am. Chem. Soc.* **2013**, *135*, 8448−8451.

(34) Zhang, Y.-Q.; Kepčija, N.; Kleinschrodt, M.; Diller, K.; Fischer, S.; Papageorgiou, A. C.; Allegretti, F.; Björk, J.; Klyatskaya, S.; Klappenberger, F.; Ruben, M.; Barth, J. V. Homo-Coupling of Terminal Alkynes on a Noble Metal Surface. *Nat. Commun.* **2012**, *3*, 1286.

(35) Gao, H.-Y.; Wagner, H.; Zhong, D.; Franke, J.-H.; Studer, A.; Fuchs, H. Glaser Coupling at Metal Surfaces. *Angew. Chem., Int. Ed.* **2013**, *52*, 4024−4028.

(36) Bringmann, G.; Gulder, T.; Gulder, T. A.; Breuning, M. Atroposelective Total Synthesis of Axially Chiral Biaryl Natural Products. *Chem. Rev.* **2011**, *111*, 563−639.

(37) Li, Q.; Yang, B.; Lin, H.; Aghdassi, N.; Miao, K.; Zhang, J.; Zhang, H.; Li, Y.; Duhm, S.; Fan, J.; Chi, L. Surface−Controlled Mono/Diselective *ortho* C−H Bond Activation. *J. Am. Chem. Soc.* **2016**, *138*, 2809−2814.

(38) Chen, Q.; Cramer, J. R.; Liu, J.; Jin, X.; Liao, P.; Shao, X.; Gothelf, K. V.; Wu, K. Steering On-Surface Reactions by a Self-Assembly Approach. *Angew. Chem.* **2017**, *129*, 5108−5112.

(39) Lin, T.; Shang, X. S.; Adisoejoso, J.; Liu, P. N.; Lin, N. Steering On-Surface Polymerization with Metal-Directed Template. *J. Am. Chem. Soc.* **2013**, *135*, 3576−3582.

(40) Zhang, R.; Lyu, G.; Li, D. Y.; Liu, P. N.; Lin, N. Template-Controlled Sonogashira Cross-Coupling Reactions on a Au(111) Surface. *Chem. Commun.* **2017**, *53*, 1731−1734.

(41) Shi, Z.; Liu, J.; Lin, T.; Xia, F.; Liu, P. N.; Lin, N. Thermodynamics and Selectivity of Two-Dimensional Metallo-Supramolecular Self-Assembly Resolved at Molecular Scale. *J. Am. Chem. Soc.* **2011**, *133*, 6150−6153.

(42) Liu, J.; Lin, T.; Shi, Z.; Xia, F.; Dong, L.; Liu, P. N.; Lin, N. Structural Transformation of Two-Dimensional Metal−Organic Coordination Networks Driven by Intrinsic In-Plane Compression. *J. Am. Chem. Soc.* **2011**, *133*, 18760−18766.

(43) Ecija, D.; Marschall, M.; Reichert, J.; Kasperski, A.; Nieckarz, D.; Szabelski, P.; Auwärter, W.; Barth, J. V. Dynamics and Thermal Stability of Surface-Confined Metal−Organic Chains. *Surf. Sci.* **2016**, *643*, 91−97.

(44) Ecija, D.; Vijayaraghavan, S.; Auwärter, W.; Joshi, S.; Seufert, K.; Aurisicchio, C.; Bonifazi, D.; Barth, J. V. Two-Dimensional Short-Range Disordered Crystalline Networks from Flexible Molecular Modules. *ACS Nano* **2012**, *6*, 4258−4265.

(45) Adisoejoso, J.; Li, Y.; Liu, J.; Liu, P. N.; Lin, N. Two-Dimensional Metallo-Supramolecular Polymerization: Toward Size-Controlled Multi-Strand Polymers. *J. Am. Chem. Soc.* **2012**, *134*, 18526−18529.

(46) Zhang, X.; Li, N.; Wang, H.; Yuan, C.; Gu, G.; Zhang, Y.; Nieckarz, D.; Szabelski, P.; Hou, S.; Teo, B. K.; Wang, Y. Influence of Relativistic Effects on Assembled Structures of V-Shaped Bispyridine Molecules on M(111) Surfaces where M = Cu, Ag, Au. *ACS Nano* **2017**, *11*, 8511−8518.

(47) Hofer, W. A. Challenges and Errors: Interpreting High Resolution Images in Scanning Tunneling Microscopy. *Prog. Surf. Sci.* **2003**, *71*, 147−183.

(48) Palotás, K.; Hofer, W. A. Multiple Scattering in a Vacuum Barrier Obtained From Real-Space Wavefunctions. *J. Phys.: Condens. Matter* **2005**, *17*, 2705−2713.

(49) Bartels, L.; Meyer, G.; Rieder, K.-H. Controlled Vertical Manipulation of Single CO Molecules with the Scanning Tunneling Microscope: A Route to Chemical Contrast. *Appl. Phys. Lett.* **1997**, *71*, 213−215.

(50) Bartels, L.; Meyer, G.; Rieder, K.-H.; Velic, D.; Knoesel, E.; Hotzel, A.; Wolf, M.; Ertl, G. Dynamics of Electron-Induced

Manipulation of Individual CO Molecules on Cu(111). *Phys. Rev. Lett.* **1998**, *80*, 2004−2007.

(51) Zhong, Q.; Ebeling, D.; Tschakert, J.; Gao, Y.; Bao, D.; Du, S.; Li, C.; Chi, L.; Schirmeisen, A. Symmetry Breakdown of 4,4″-Diamino-p-Terphenyl on a Cu (111) Surface by Lattice Mismatch. *Nat. Commun.* **2018**, *9*, 3277.

(52) Kawai, S.; Haapasilta, V.; Lindner, B. D.; Tahara, K.; Spijker, P.; Buitendijk, J. A.; Pawlak, R.; Meier, T.; Tobe, Y.; Foster, A. S.; Meyer, E. Thermal Control of Sequential On-Surface Transformation of a Hydrocarbon Molecule on a Copper Surface. *Nat. Commun.* **2016**, *7*, 12711.

(53) Kawai, S.; Takahashi, K.; Ito, S.; Pawlak, R.; Meier, T.; Spijker, P.; Canova, F. F.; Tracey, J.; Nozaki, K.; Foster, A. S.; Meyer, E. Competing Annulene and Radialene Structures in a Single Anti-Aromatic Molecule Studied by High-Resolution Atomic Force Microscopy. *ACS Nano* **2017**, *11*, 8122−8130.

(54) Wang, T.; Lv, H.; Feng, L.; Tao, Z.; Huang, J.; Fan, Q.; Wu, X.; Zhu, J. Unravelling the Mechanism of Glaser Coupling Reaction on Ag(111) and Cu(111) Surfaces: A Case for Halogen Substituted Terminal Alkyne. *J. Phys. Chem. C* **2018**, *122*, 14537−14545.

(55) Mao, X. F.; Lin, T.; Adisoejoso, J.; Shi, Z.; Shang, X. S.; Liu, P. N.; Lin, N. Coordination Self-Assembly of Bromo-Phenyl and Pyridyl Functionalized Porphyrins with Fe on an Au (111) Surface. *Phys. Chem. Chem. Phys.* **2013**, *15*, 12447−12450.

(56) Shi, Z.; Lin, N. Structural and Chemical Control in Assembly of Multicomponent Metal−Organic Coordination Networks on a Surface. *J. Am. Chem. Soc.* **2010**, *132*, 10756−10761.

(57) Lin, T.; Kuang, G.; Shang, X. S.; Liu, P. N.; Lin, N. Self-Assembly of Metal−Organic Coordination Networks Using On-Surface Synthesized Ligands. *Chem. Commun.* **2014**, *50*, 15327−15329.

(58) Fan, Q.; Werner, S.; Tschakert, J.; Ebeling, D.; Schirmeisen, A.; Hilt, G.; Hieringer, W.; Gottfried, J. M. Precise Mono-Selective Aromatic C−H Bond Activation by Chemisorption of Meta-Aryne on a Metal Surface. *J. Am. Chem. Soc.* **2018**, *140*, 7526−7532.

(59) Kresse, G.; Hafner, J. *Ab initio* Molecular Dynamics for Liquid Metals. *Phys. Rev. B: Condens. Matter Mater. Phys.* **1993**, *47*, 558−561.

(60) Kresse, G.; Furthmüller, J. Efficient Iterative Schemes for *ab initio* Total-Energy Calculations Using a Plane-Wave Basis Set. *Phys. Rev. B: Condens. Matter Mater. Phys.* **1996**, *54*, 11169−11186.

(61) Kresse, G.; Furthmüller, J. Efficiency of *ab initio* Total Energy Calculations for Metals and Semiconductors Using a Plane-Wave Basis Set. *Comput. Mater. Sci.* **1996**, *6*, 15−50.

(62) Blöchl, P. E. Projector Augmented-Wave Method. *Phys. Rev. B: Condens. Matter Mater. Phys.* **1994**, *50*, 17953−17979.

(63) Klimeš, J.; Bowler, D. R.; Michaelides, A. Chemical Accuracy for the van der Waals Density Functional. *J. Phys.: Condens. Matter* **2010**, *22*, 022201.

(64) Lee, K.; Murray, É. D.; Kong, L.; Lundqvist, B. I.; Langreth, D. C. Higher-Accuracy van der Waals Density Functional. *Phys. Rev. B: Condens. Matter Mater. Phys.* **2010**, *82*, 081101.

(65) Klimeš, J.; Bowler, D. R.; Michaelides, A. Van der Waals Density Functionals Applied to Solids. *Phys. Rev. B: Condens. Matter Mater. Phys.* **2011**, *83*, 195131.